Physica Scripta

PAPER

Escape from the potential well: accelerating by shaping and noise tuning

Bartłomiej Dybiec and Mikołaj Zawiślak

Institute of Theoretical Physics, and Mark Kac Center for Complex Systems Research, Jagiellonian University, ul. St. Łojasiewicza 11, 30–348 Kraków, Poland

E-mail: bartlomiej.dybiec@uj.edu.pl

Keywords: mean first passage time, Lévy noise, noise induced escape, stochastic dynamics

OPEN ACCESS

RECEIVED
23 August 2022

REVISED
19 December 2022

ACCEPTED FOR PUBLICATION
18 January 2023

PUBLISHED
30 January 2023

Abstract

Noise driven escape from the potential well is the basic component of various noise induced effects. The efficiency of the escape process or time scales matching is responsible for occurrence of the stochastic resonance and (stochastic) resonant activation. Here, we are extending the discussion on how the structure of the potential can be used to optimize the mean first passage time. It is demonstrated that corrugation of the potential can be beneficial under action of the weak Gaussian white noise. Furthermore, we show that the noise tuning can be more effective than shaping the potential. Therefore, action of the tuned additive α-stable noise can accelerate the escape kinetics more than corrugation of the potential. Finally, we demonstrate that mean first passage time from a potential well can be a non-monotonous function of the stability index α.

1. Introduction

Stochastic resonant activation [1, 2] and stochastic resonance [3–5] changed our perception of noise [4]. These two seminal effects have indicated that efficiency of some processes depends on noise—optimal dose of noise can significantly increase system efficiency, as measured by mean first passage time, or input output synchronization. These effects play an important role not only as theoretical concepts but also in real life situations and biological realms [6–8].

In the overdamped regime, without a noise, a particle cannot surmount the potential barrier. Therefore, the escape from the potential well is possible due to the action of noise only. The mean first passage time is one of the main quantities which characterizes escape kinetics. The escape from the potential well [9, 10] underlines various noise induced effects. In (stochastic) resonant activation [1] a modulation of the potential barrier is used to minimize the mean first passage time, while in the stochastic resonance [3, 4] the noise is used to amplify weak signal by fine-tuning time scales associated with the noise driven escape and external modulation. Analogously, in ratchets [11], the motion in periodic potential, assumes multiple escapes from sequence of periodic potential wells.

The noise driven dynamics in the static potentials is sensitive to the shape and structure of the potential [12–14]. In ratchets [15, 16], it has been demonstrated that the corrugated structure of the potential can increase the efficiency of the ratcheting devices [17, 18]. It indicates that the mean first passage time depends not only on the potential shape but also on its internal structure [19]. Superimposed corrugation [20] on the potential profile can be used to modify the escape rate.

Typically it is assumed that the noise is Gaussian and white [21], which is the natural consequence of the large number of statistically independent interactions of a test particle with other molecules which are bounded in time. Nevertheless, various non-Gaussian and non-white extensions have been suggested [22, 23]. One can assume that noise is still white but follow a more general power-law, heavy-tailed distributions, often of the α-stable Lévy type [24, 25, 23], what resembles the transition from the central limit theorem to the generalized central limit theorem [26, 27]. The white Lévy noise naturally appears in descriptions of out-of-equilibrium systems. It breaks the microscopic reversibility [28] and changes properties of stationary states of systems

compared to their equilibrium counterparts [29, 30]. Classical examples of systems displaying heavy-tailed fluctuations of the α-stable type includes, but are not limited to, turbulent fluid flows [31–34], magnetized plasmas [35, 36], optical lattices [37], heartbeat dynamics [38], neural networks [39], search on a folding polymers [40], animal movement [41], climate dynamics [42], financial time series [43], spreading of diseases and dispersal of banknotes [44]. α-stable variables are also used in financial markets [45], portfolio optimization [46] and neuroscience [47, 48].

Here, we explore how the corrugation of the potential, modeled as superimposed oscillations [20], affect the mean first passage time from an interval restricted by two absorbing boundaries. In particular, we compare the gain due to corrugation of the potential with yield due to noise tuning as we relax the assumption that the motion is driven by the Gaussian white noise. The more general noise of the α-stable type [23] can be used to modify the mean first passage time from a potential well. The model under study is described and analyzed in the next section (section 2 Model and Results). The manuscript is closed with Summary and Conclusions (section 3).

2. Model and Results

The (overdamped) Langevin equation [49–51]

$$\frac{dx}{dt} = -V'(x) + \sigma\xi(t), \tag{1}$$

is used as an efficient tool to describe stochastic dynamics. In equation (1), $x(t)$ represents the particle position, $-V'(x)$ stands for the deterministic force while $\xi(t)$ represents the random forces modeled here by the zero mean and delta correlated Gaussian white noise

$$\langle\xi(t)\rangle = 0 \qquad \text{and} \qquad \langle\xi(t)\xi(s)\rangle = \delta(t-s). \tag{2}$$

The overdamped Langevin equation is the strong friction limit of the full (underdamped) Langevin equation [52, 53], which is obtained via the adiabatic elimination of the fast variables [21]. The problem of dimensionality of the (overdamped) Langevin equation is discussed in the appendix. Examination of the Langevin equation underlines studies on noise induced effects like (stochastic) resonant activation [1], stochastic resonance [3, 4], noise enhanced stability [54] to name a few.

In the overdamped regime, in the absence of stochastic force the system is fully determined by the deterministic force. The observed dynamics is especially simple—if there are local minima of the potential—a particle deterministically slides towards one of them or moves towards infinity. After reaching a local minimum it stands there forever. The situation drastically changes in the presence of noise. Action of noise can result in a noise induced escape. Now, minima of the potential are not absolutely stable—deeper minima are more stable because it is harder to leave them. Under action of the Gaussian white noise, the mean time to escape from the potential well grows exponentially with the barrier height.

We study the problem of the first escape from the finite interval under combined action of the deterministic and random forces. The first escape is characterized by the mean first passage time (MFPT) which is the average of first passage times, i.e. times needed to leave the domain of motion Ω for the first time

$$\mathcal{T} = \langle t_{\text{fp}}\rangle = \langle \min\{t\colon x(0) = x_0 \ \wedge \ x(t) \notin \Omega\}\rangle, \tag{3}$$

where x_0 is the initial position ($x_0 \in \Omega$). For example, for escape from the interval $[a, b]$ restricted by two absorbing boundaries the mean first passage time reads [21]

$$\mathcal{T}_{\text{th}}(x) = \frac{2}{\int_a^b \frac{dy}{\psi(y)}}\left[\left(\int_a^x \frac{dy}{\psi(y)}\right)\int_x^b \frac{dy'}{\psi(y')}\int_a^{y'}\frac{\psi(z)}{\sigma^2}dz - \left(\int_x^b \frac{dy}{\psi(y)}\right)\int_a^x \frac{dy'}{\psi(y')}\int_a^{y'}\frac{\psi(z)}{\sigma^2}dz\right], \tag{4}$$

where x is the initial position ($a \leqslant x \leqslant b$) and $\psi(x) = \exp(-2V(x)/\sigma^2)$. Considering symmetries, under action of the Gaussian white noise, for $x = 0$, $a = -b$ and even $V(x)$, i.e. $V(x) = V(-x)$, the escape from the interval restricted by two absorbing boundaries is equivalent to the escape from the interval restricted by reflecting boundary at $a = 0$ and the absorbing boundary at b ($b > 0$). In such a case the MFPT reads

$$\mathcal{T}_{\text{th}}(x = 0) = 2\int_0^b \frac{dy}{\psi(y)}\int_0^y \frac{\psi(z)}{\sigma^2}dz. \tag{5}$$

The MFPT is fully determined by barrier type, barrier position, starting point and the potential, see equations (4) and (5).

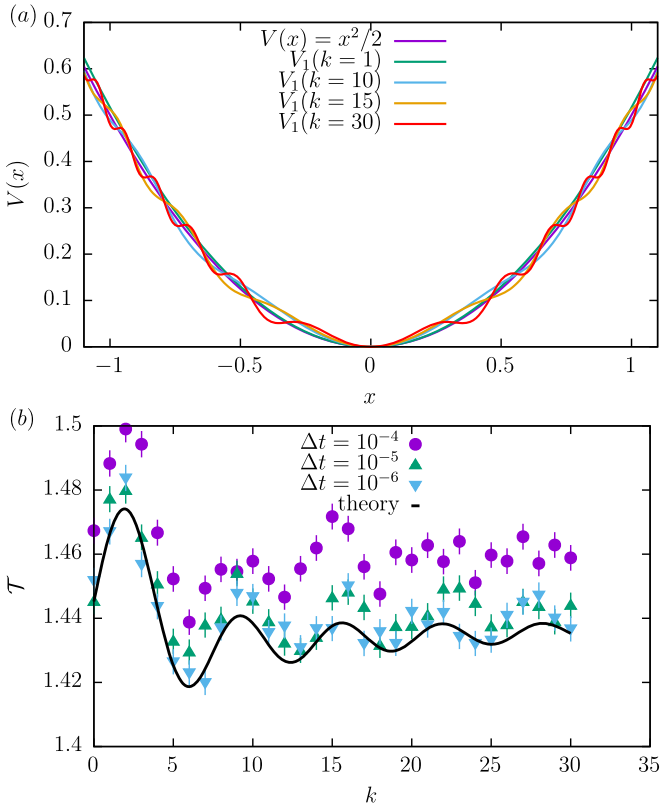

Figure 1. The corrugated potential $V_1(x)$, see equation (6), for various values of the control (corrugation) parameter k (top panel—(*a*)), obtained values of the MFPT (bottom panel—(*b*)). Solid line in the bottom panel shows the theoretical value of the MFPT, see equation (4). Absorbing boundaries are located at ± 1, while the scale parameter σ is set to unity. Numerical results, see equations (3) and (11) have been averaged over 10^5 realizations. Various points correspond to different values of the integration time step Δt. Error bars represent the standard deviation of the mean.

Here we assume that the potential well is not fully smooth, but it has the internal structure in the form of superimposed oscillations. The potential $V(x)$ is corrugated, i.e. on the dominating $x^2/2$ profile ripples are added. For that purpose we use

$$V_1(x) = \frac{x^2}{2} + \frac{\sin(kx^2)}{50}, \tag{6}$$

and

$$V_2(x) = \frac{x^2}{2} + \frac{\sin(kx^2)\exp(-5x^2)}{10}. \tag{7}$$

For both potentials k is the parameter controlling the corrugation level. For $k = 0$, $V_1(x)$ and $V_2(x)$ reduce to the harmonic potential $V(x) = x^2/2$. Exemplary potentials $V_1(x)$ and $V_2(x)$ corresponding to various values of the corrugation parameter k are presented in top panels of figures 1 and 2. Potentials $V_1(x)$ and $V_2(x)$ differ by the corrugation type. For $V_1(x)$ corrugations are undamped, i.e. superimposed oscillations are of the same order, while for $V_2(x)$ they are exponentially damped with the increasing distance from the origin, c.f., figures 1(a) and 2(a). For setups studied in figures 1 and 2 absorbing boundaries are located at ± 1, while the scale parameter σ is set to $\sigma = 1$.

From equation (4) one can calculate the MFPT from $[-1, 1]$ for the noise driven motion in the deterministic potential $V_1(x)$ and $V_2(x)$. Theoretical dependence of the MFPT is plotted with the solid line in bottom panels of figures 1 ($V_1(x)$) and 2 ($V_2(x)$). For $V_1(x)$, as a function of the corrugation parameter k, the MFPT displays multiple local minima and maxima as its shape resembles damped oscillations. These multiple minima could be attributed to the corrugation induced locking, in a manner similar to emergence of non-equilibrium stationary states [55]. For $V_2(x)$ the MFPT is a non-monotonous function of k with a minimum at $k \approx 18.2$. Theoretical dependence of MFPT clearly demonstrates that the corrugation parameter k can be used to optimize the process of the first escape. The internal structure of the potential builds steps/micro-wells like structure which simultaneously helps climbing up the potential and weakens the deterministic sliding [17]. Now, instead of sliding to the global minimum ($x = 0$) a particle slides to the nearest local minimum, which can be left due to the action of the noise only. Therefore, for the motion in the corrugated potential, it is harder to lose reached

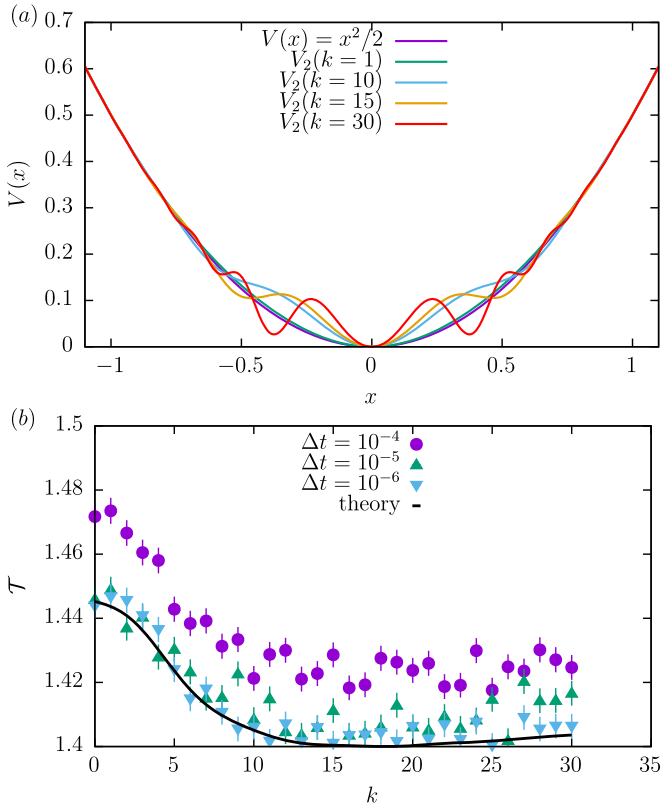

Figure 2. The same as in figure 1 for the $V_2(x)$ potential, see equation (7).

'height'. Figures 1(b) and 2(b) indicate that the corrugation of the potential can be used for optimization of the first escape process. Therefore, among considered values of the parameter k controlling the level of corrugation there are such values which result in the fastest escape process as measured by the MFPT. For $V_1(x)$ extrema of MFPT (starting with the maximum) are approximately recorded at $k \in \{1.92, 5.99, 9.22, 12.39, 15.6, 18.72, 21.93, 25.1, 28.21\}$. Interestingly for $V_1(x)$ with $k > 5$ extrema of MFPTs are recorded at k values that do not change the height of the potential barrier measured at the absorbing boundary ($x = 1$), i.e. $V_1(x)|_{x=1} = \frac{1}{2}$. Therefore, decrease or increase of the MFPT (except $k \approx 1.92$ case) cannot be attributed to lowering or increasing the potential barrier. Moreover, exploration of $V_1(x)$ has revealed that minima of the MFPT are recorded when the last bending is convex. At the same time maxima are recorded when the last bending is concave. When the final bending is convex it builds a step which allows for additional accumulation of the probability mass closer to the absorbing boundary. Contrary to $V_1(x)$, exploration of the first escape process from $V_2(x)$ indicates a different source of optimization as the damping term $\exp(-5x^2)$ makes final parts of the potential well practically k independent. Therefore, the problem of optimization of the escape kinetics calls for further studies.

In figures 1(b) and 2(b) in addition to theoretical values of the MFPT $\mathcal{T}_{\text{th}}$, see equation (4), results of computer simulations are presented. In order to estimate first passage time we simulate the Langevin equation (1) using the Euler-Maruyama scheme (11) until absorption at the absorbing boundaries located at $x = \pm b = \pm 1$. From the ensemble of estimated first passage times we calculate the mean first passage time and its error (standard deviation of the mean). Points in figures 1(b) and 2(b) represent results of computer simulations with varying the integration time step $\Delta t \in \{10^{-4}, 10^{-5}, 10^{-6}\}$ and averaged over 10^5 realizations, but we have also verified that averaging over 10^4 realizations produces statistically same results.

For $\sigma = 1$, results corresponding to $\Delta t = 10^{-4}$ reconstruct the dependence of the MFPT, but the level of agreement is not very good. Decrease in the integration time step improves the level of agreement and makes it sufficient. Nevertheless, the problem is hard to tackle numerically. Subsequent figure 3 shows the ratio between numerically obtained and theoretical results, namely

$$\left| \frac{\mathcal{T}}{\mathcal{T}_{\text{th}}} - 1 \right| \times 100\ [\%], \tag{8}$$

for both potentials $V_1(x)$ (top panel) and $V_2(x)$ (bottom panel). From figure 3 it is clearly visible that already for $\Delta t = 10^{-4}$ the relative errors are smaller than 2.5%. The decrease of the integration time step decreases the

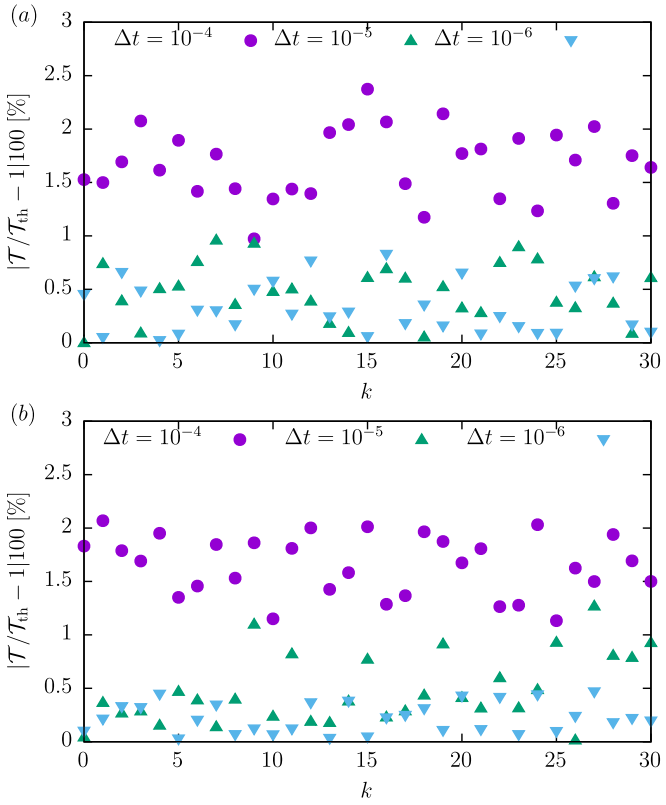

Figure 3. The ratio between theoretical $\mathcal{T}_{\rm th}$ and numerically approximated MFPTs $\mathcal{T}$ for $V_1(x)$ (top panel—(*a*)) and $V_2(x)$ (bottom panel—(*b*)) as a function of k, see figures 1 and 2. Various curves depict results with different integration time steps Δt. Results have been averaged over 10^5 realizations.

relative errors well below 1%. Moreover, for $\Delta t = 10^{-6}$ the relative errors are slightly smaller than for $\Delta t = 10^{-5}$. The problem of reconstruction of theoretical results by methods of stochastic dynamics originates in the fact that minima of MFPT, as a function of the corrugation parameter k, are very shallow. Exact values of the MFPT can be calculated by use of equations (4) and (5). For instance, for $V_1(x)$, the minimal MFPT, i.e. $\min_k\{\mathcal{T}_{\rm th}\}$, is smaller than the MFPT for the non corrugated potential, i.e. $\mathcal{T}_{\rm th}(k = 0)$, by 1.8%, while for $V_2(x)$ it is 3.1%, but this time the minimum is not very well localized and separated from MFPTs at large k values. For that reason, the very high precision of simulations is required. In order to increase accuracy it is necessary to decrease the time step of integration and increase the number of repetitions. However, within the used class of potentials, the decrease in MFPT due to the structure of the potential is minimal. Nevertheless, one can play with the model parameters. For instance, for the same potentials decrease of σ from 1 to 0.5 results in a stronger effect, i.e. due to potential roughening MFPT can be reduced by 11.8% for $V_1(x)$ and by 15.1% for $V_2(x)$ what can be verified by numeric evaluation of the integral (5). Smaller acceleration is observed for the potential $V_1(x)$, because superimposed oscillations are undamped and they produce deeper local minima of the potential, which are harder to escape from. Contrary to the potential $V_1(x)$ for $V_2(x)$ corrugations are damped and consequently local minima are shallower. They still act as steps but now these steps do not introduce (strong) additional trapping like for $V_1(x)$ On the one hand, numerical evaluation of equation (5) gives trustworthy results and can be used to assess the role of potential roughening on the optimization of the escape kinetics under action of the Gaussian white noise. On the other hand, we are interested in verifying if a change of the driving noise type can be more beneficial than shaping of the potential. Therefore, in the next step we exchange the Gaussian white noise in equation (1) by the symmetric α-stable noise [23] to check if noise tuning can be more beneficial than corrugation of the potential. Trajectories of overdamped processes driven by α-stable noises are discontinuous [24, 27]. A particle driven by Lévy noise does not need to hit the boundary but it can jump over it [56]. The possibility of not visiting intermediate points due to long jumps makes the escape scenario different than for the Gaussian white noise driving [57–59], which is going to be explored in more details in the further part of the manuscript. Contrary to the Gaussian driving, under Lévy noise the barrier width is more important than its height [57–59].

The α-stable noise is a generalization of the Gaussian white noise to the nonequilibrium realms [24], where heavy tailed fluctuations are abundant [42, 60–65]. The noise produces independent increments which follow a heavy-tailed α-stable density [24, 27]. The symmetric α-stable noise is the formal time derivative of the symmetric α-stable process $L(t)$, see [23, 24]. Increments, $\Delta L = L(t + \Delta t) - L(t)$, of the symmetric α-stable

process $L(t)$ are stationary, independent and identically distributed according to the α-stable density. Symmetric α-stable distributions are defined by the characteristic function [24, 27]

$$\varphi(k) = \langle e^{ikx} \rangle = \exp\left[-\sigma_0^\alpha |k|^\alpha / 2\right], \tag{9}$$

where σ_0 is the scale parameter. Without loss of generality, within the manuscript we use $\sigma_0 = 1$, because the scale parameter σ_0 can be incorporated into the fluctuation strength σ in equation (1). The characteristic function (9) is a slightly modified [26, 66] standard form of the characteristic function of α-stable densities. Such an amendment assures that for $\alpha = 2$ the Gaussian white noise with $\langle \xi(t)\xi(s) \rangle = \delta(t-s)$ is recovered, see equation (1). Therefore, for $\alpha = 2$, the characteristic function of α-stable densities, see equation (9), reduces to the characteristic function of the normal distribution $N(0,\ \sigma_0^2) = N(0,\ 1)$.

Increments ΔL are distributed according to the unimodal probability density with the characteristic function $\langle e^{ik\Delta L} \rangle = \exp\left[-\Delta t \sigma_0^\alpha |k|^\alpha / 2\right]$. The stability index α ($0 < \alpha \leqslant 2$) controls the asymptotics of the distribution, which for $\alpha < 2$ is of power-law type $p(x) \propto |x|^{-(\alpha+1)}$. The scale parameter σ_0 ($\sigma_0 > 0$) determines the width of the distribution, which can be defined by an interquantile width or by fractional moments, i.e. $\langle |x|^\nu \rangle$ with $\nu < \alpha$, because the variance of α-stable variables with $\alpha < 2$ diverges. The scale parameter σ_0 in equation (9) and fluctuation strength σ in equation (1) play the same role. More precisely, setups $\{\sigma_0 = \sigma, \sigma = 1\}$ and $\{\sigma_0 = 1, \sigma = \sigma\}$ are equivalent. Consequently, without loss of generality, σ_0 can be set to unity and the width of theα-stable distribution is controlled by the strength of fluctuations σ. From general theory, it implies that an α-stable process $L(t)$ can be decomposed [67–69] into a compound Poisson process that describes long jumps and the Wiener part responsible for small displacements. Possibility of long jumps makes the MFPT more dependent on the barrier width [57–59] than its height [21], which is the main factor determining the MFPT under Gaussian white noise driving.

Trajectories of processes driven by α-stable noise are no longer continuous [24]. Therefore, systems driven by such a noise do not display the property present for Gaussian white noise allowing for transformation of equation (4) into equation (5), i.e. absorbing-absorbing setup cannot be replaced by the reflecting-absorbing one. Moreover, analytical results for systems driven by Lévy noise are very limited. The general formula for the escape of a free particle from $[-L, L]$ interval reads [70–74]

$$\mathcal{T}(x) = \frac{1}{\Gamma(1+\alpha)} \frac{(L^2 - x^2)^{\alpha/2}}{(\sigma/\sqrt{2})^\alpha}. \tag{10}$$

The $\sqrt{2}$ factor in the denominator comes from the used form of the characteristic function, see equation (9). For $x = 0$, the MFPT reduces to $\mathcal{T}(0) = [L/(\sigma/\sqrt{2})]^\alpha / \Gamma(1+\alpha)$. The scaling of the MFPT on the scale parameter σ and the interval width can be deducted from arithmetic properties of α-stable distributions [75]. In more general cases than escape from a finite interval some scaling [76] or weak noise limits [77, 78] are known. Therefore, we continue studies on the MFPT, see equation (3), numerically. The Langevin equation, see equation (1), is approximated by the (stochastic) Euler–Maruyama method [79, 80]

$$x(t+\Delta t) = x(t) - V'(x)\Delta t + \sigma \Delta t^{1/\alpha} \xi_\alpha^t. \tag{11}$$

In equation (11) ξ_α^t represents the sequence of independent identically distributed α-stable random variables which can be generated using well-known algorithms [81–83]. The Gaussian white noise is recovered for $\alpha = 2$, see [27], and the Euler-Maruyama scheme attains the standard form [84]. Figure 4 presents results for the MFPT under action of α-stable noise for a particle moving in $V_1(x)$ (top panel) and $V_2(x)$ (bottom panel) as a function of the corrugation parameter k. Various curves correspond to different values of the stability index α ($\alpha \in \{0.5, 0.75, 1, 1.25, 1.5, 1.75, 2.0\}$). The scale parameter σ is set to $\sigma = 1$. In addition to $\alpha = 2$, for $V_1(x)$ with $\alpha \in \{0.75, 1, 1.25\}$, the weak periodicity of MFPT is visible, see figure 4(a). Actually, for $\alpha = 0.75$ local minima of MFPT are (relatively) deeper than for the Gaussian white noise. Importantly, the MFPT is more sensitive to the value of the stability index α than to the structure of the potential as the curves corresponding to various values of the stability index α are spread along the figures, c.f., figure 4.

For the escape of a Lévy noise driven free particle from a finite interval [70, 72–74, 85] the MFPT can be a non-monotonous function of the stability index α, see [86]. Therefore, one can expect a similar behavior for a particle moving in a deterministic potential, see figure 5. Due to the action of the deterministic, restoring force, recorded values of the MFPT are significantly larger than for a free particle. For studied setups, the MFPT is a non-monotonous function of the stability index α. Therefore, it is possible to find such α which minimizes MFPT. In the models under study it is $\alpha = 2$ (Gaussian white noise) and $\alpha = 0.5$ (heavy tailed, non-equilibrium noise). Maximal values of MFPT, for both setups $V_1(x)$ and $V_2(x)$, are recorded for $\alpha \approx 1.25$. Figure 5 clearly indicates that it can be more beneficial to optimize the α-stable noise type (α) than the potential structure (k). Accidentally, the Gaussian white noise, which we started with, resulted in the minimal MFPT. Figure 5 confirms that variability in the MFPT due to change of α is significantly larger than the spread due to the corrugation

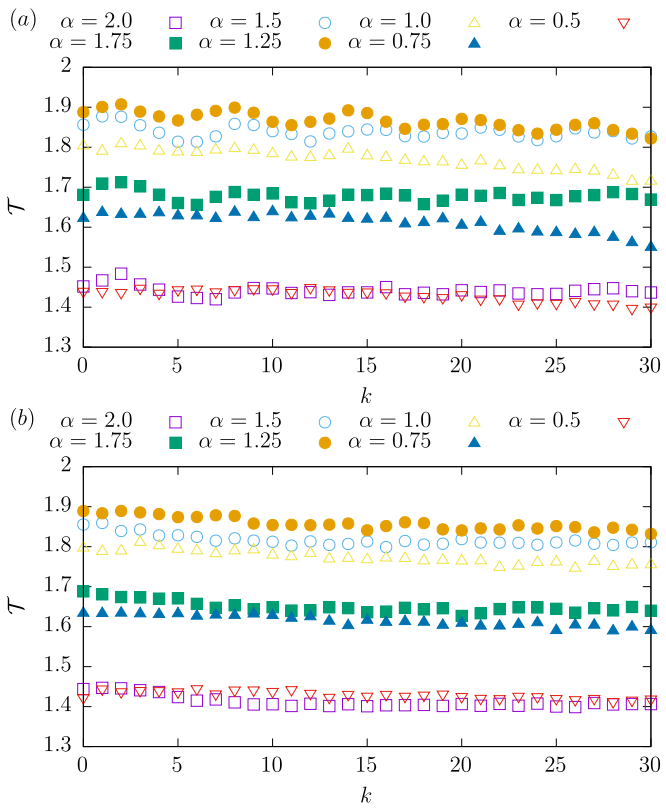

Figure 4. MFPT for $V_1(x)$ (top panel—(*a*)) and $V_2(x)$ (bottom panel—(*b*)) as a function of the corrugation parameter k. Various curves correspond to different α-stable noises, see equation (9). Results have been constructed numerically, see equations (3) and (11), with $\Delta t = 10^{-6}$ and averaged over 10^5 realizations.

parameter k. Moreover, except $\alpha = 2$ case, recorded MFPT do not differ between both setups $V_1(x)$ and $V_2(x)$ significantly, see figures 5(a) and (b).

Using formula (10) it can be demonstrated that for a free particle the MFPT can be not only a non-monotonous function of the stability index α, see [86], but it can change its monotonicity depending on σ. Therefore, finally, we have repeated some of the simulations with other values of σ in order to see differences and similarities between escape kinetics from finite intervals and the potential well. The case of $\alpha = 2$ can be studied with use of equation (5), while $\alpha < 2$ needs to be analyzed numerically. Not surprisingly, the inspection of equation (5) shows that for the Gaussian white noise with decreasing σ corrugation plays an increasing role. Nevertheless, changes in the recorded values of the MFPT caused by the noise type dominate over amendments produced by the potential roughening. Furthermore, as for $\sigma = 1$ results for $V_1(x)$ and $V_2(x)$ are very similar, we present additional results, see figure 6, for $V_1(x)$ only, see figure 1. Despite the fact that decrease in σ can make MFPT more sensitive to corrugation optimization, in the studied cases we have observed larger spread of MFPT values due to noise type, than corrugation strength, see figure 6. Figure 6 presents mean first passage time $\mathcal{T}$ as a function of the stability index α. Various points correspond to different values of the corrugation parameter k. Various panels (*a*)—(*f*) display results for different values of the scale parameter σ ($\sigma \in \{0.5,\ 1,\ \sqrt{2},\ 2,\ 4,\ 16\}$). Additional solid lines in each panel depict the mean first passage time of a free particle from a finite interval, see equation (10). Spread of results with a fixed value of the stability index α is produced by the corrugation of the potential, which is particularly well visible for $\alpha = 2$ and small σ, e.g. $\sigma = 0.5$. Especially at low values of σ, corrugation of the potential can be used for fine-tuning of escape kinetics, but a more important role is played by the adjustment of the noise type, i.e. the exponent α. The change in σ not only changes recorded values, but also modifies monotonicity of $\mathcal{T}(\alpha)$ in an analogous way like for the escape of a free particle from a finite interval, see [86]. In the large σ limit, e.g. $\sigma \in \{4, 16\}$, a particle practically does not feel the deterministic force and the MFPT approaches the MFPT of a free particle from a finite interval, see equation (10). For moderate and small σ, escape from the potential well is visibly slower than escape from a finite interval. These results are not only coherent with studies on the escape from a finite interval but also on the escape from a potential well [76], indicating that the escape kinetics is affected by the scale parameter σ.

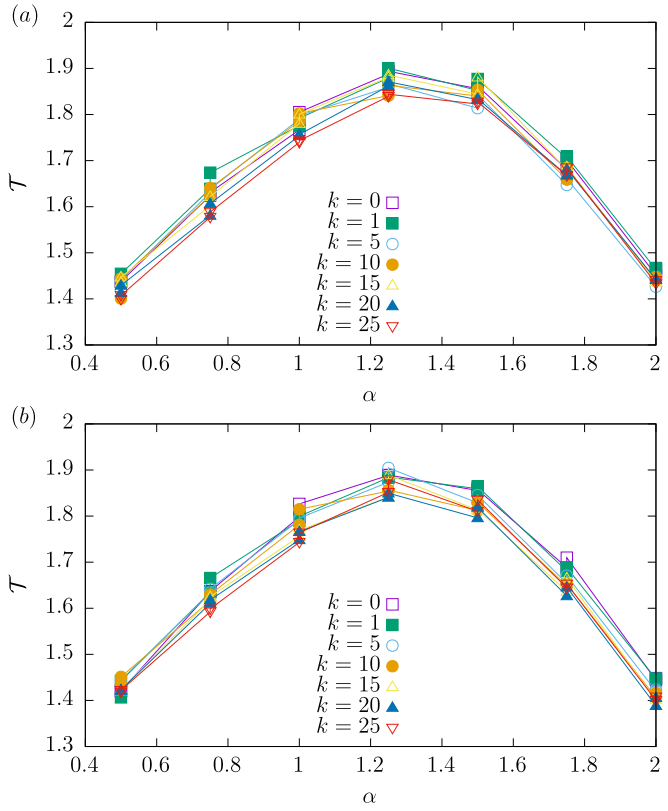

Figure 5. MFPT for $V_1(x)$ (top panel—(*a*)) and $V_2(x)$ (bottom panel—(*b*)) as a function of the stability index α. Various curves correspond to different corrugations of the potential. Results have been constructed numerically, see equations (3) and (11), with $\Delta t = 10^{-6}$ and averaged over 10^5 realizations.

3. Summary and conclusions

The mean first passage time is an important quantifier characterizing efficiency of the noise driven dynamics. MFPT can be optimized in numerous ways, like shaping of the potential and noise tuning. Here, we have demonstrated that the internal structure of the potential produced by the additional corrugation superimposed on the potential profile can be used to decrease the MFPT. Nevertheless, the decrease in the MFPT does not need to be significant. It turned out that tuning of the α-stable noise can be more beneficial than corrugation of the potential. The type of the optimal noise is sensitive to the noise strength measured by the scale parameter σ. For small σ fastest escape is recorded at lowest values of the stability index α, while for large σ, Gaussian white noise produces the fastest escape. There is also an intermediate range, with minima recorded at small and $\alpha = 2$ drivings. Finally, we have verified that for strong noise (large σ) the escape kinetics approaches the one of a free particle from a finite interval.

Acknowledgments

This research was supported in part by PLGrid Infrastructure. The research for this publication has been supported by a grant from the Priority Research Area DigiWorld under the Strategic Programme Excellence Initiative at Jagiellonian University.

Data availability statement

The data that support the findings of this study are available upon reasonable request from the authors.

Appendix. Units in the Langevin equation

Units in the Langevin equation can be established from general physical principles [21, 52] like equipartition theorem or from probabilistic considerations. Both approaches are fully coherent. We start with the use of the

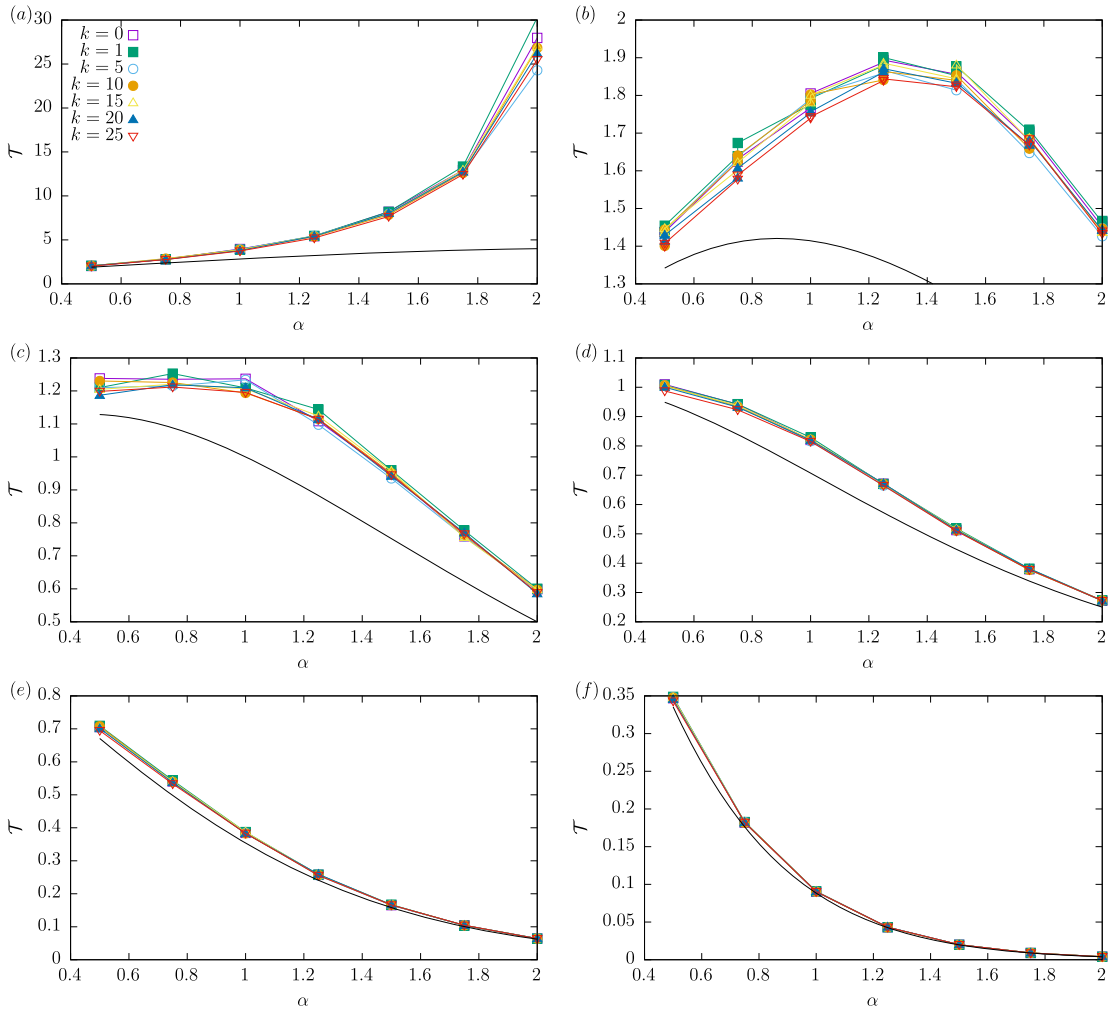

Figure 6. Dependence of the mean first passage time $\mathcal{T}$ on the stability index α. Various points correspond to different values of the corrugation parameter k, while various panels (a)—(f) represent different values of the scale parameter σ ($\sigma \in \{0.5,\ 1,\ \sqrt{2},\ 2,\ 4,\ 16\}$). The solid lines show the MFPT from the finite interval, see equation (10).

following (overdamped) Langevin equation [50]

$$\dot{x}(t) = \frac{f(x)}{\gamma} + \sigma\xi(t), \tag{A.1}$$

where: x—is a position of the particle, γ—stands for a friction coefficient, σ—represents strength of the noise and $\xi(t)$—is the α-stable, Lévy type white noise characterized by the stability index α ($\alpha \in (0, 2]$). The force $f(x)$ acting on a particle is determined by the external potential, $f(x) = -dV(x)/dx$. Corresponding units in equation (A.1) are: $[x] = [\text{length}]$, $[\gamma] = [\text{mass}]/[\text{time}]$, $[f(x)] = [V'(x)] = [\text{mass}] \times [\text{length}]/[\text{time}]^2 = [\text{force}]$, $[V(x)] = [\text{force}] \times [\text{length}] = [\text{energy}]$, $[\sigma] = [\text{length}]/[\text{time}]^{1/\alpha}$ and $[\xi(t)] = 1/[\text{time}]^{1-1/\alpha}$. Stability index α is dimensionless. In the asymptotic limit of $\alpha = 2$ the Lévy white noise is equivalent to the Gaussian white noise and it has standards units, i.e. $[\xi_{\alpha=2}(t)] = 1/\sqrt{[\text{time}]}$. Moreover, in an alternative approach, the strength of fluctuation σ can be transformed into the diffusion constant $D \propto \sigma^{\alpha}$, see [25, 76, 87]. For $\alpha = 2$, the diffusion constant is related to the system temperature and friction $D = k_B T/\gamma$ by the Einstein-Smoluchowski-Sutherland relation. For a free particle (with $\alpha = 2$) $\langle [x(t) - x(0)]^2(t) \rangle = 2Dt$. For $\alpha < 2$, the friction and the strength of fluctuations are two independent parameters. Furthermore, the mean square displacement diverges. The MFPT given by equation (10) is measured in units of time. Finally, the Langevin equation (1) is obtained from equation (A.1) by setting $\gamma = 1$.

ORCID iDs

Bartłomiej Dybiec https://orcid.org/0000-0002-6540-3906

References

[1] Doering C R and Gadoua J C 1992 *Phys. Rev. Lett.* **69** 2318–21
[2] Spalding C, Doering C R and Flierl G R 2017 *Phys. Rev.* E **96** 042411
[3] McNamara B and Wiesenfeld K 1989 *Phys. Rev.* A **39** 4854–69
[4] Gammaitoni L, Hänggi P, Jung P and Marchesoni F 2009 *Eur. Phys. J.* B **69** 1–3
[5] Krauss P, Metzner C, Schilling A, Schütz C, Tziridis K, Fabry B and Schulze H 2017 *Sci. Rep.* **7** 1–8
[6] Simonotto E, Riani M, Seife C, Roberts M, Twitty J and Moss F 1997 *Phys. Rev. Lett.* **78** 1186
[7] Russell D F, Wilkens L A and Moss F 1999 *Nature* **402** 291–4
[8] Hänggi P 2002 ChemPhysChem **3** 285–90
[9] Farkas L 1927 *Z. Chem. Phys. (Leipzig)* **125** 236–42
[10] Kramers H A 1940 *Physica (Utrecht)* **7** 284
[11] Astumian R D 1997 *Science* **276** 917–22
[12] Dellago C, Bolhuis P and Geissler P L 2002 *Adv. Chem. Phys.* **123** 1–78
[13] Palyulin V V and Metzler R 2012 *J. Stat. Mech.J. Stat. Mech.* **2012** L03001
[14] Chupeau M, Gladrow J, Chepelianskii A, Keyser U F and Trizac E 2020 *Proc. Natl. Acad. Sci. U.S.A.* **117** 1383–8
[15] Magnasco M O 1993 *Phys. Rev. Lett.* **71** 1477–81
[16] Reimann P 2002 *Phys. Rep.* **361** 57–265
[17] Li Y, Xu Y, Kurths J and Yue X 2017 *Chaos* **27** 103102
[18] Li Y, Xu Y and Kurths J 2017 *Phys. Rev.* E **96** 052121
[19] Li Y, Xu Y, Kurths J and Yue X 2016 *Phys. Rev.* E **94** 042222
[20] Zwanzig R 1988 *Proc. Natl. Acad. Sci. U.S.A.* **85** 2029–30
[21] Gardiner C W 2009 *Handbook of Stochastic Methods for Physics, Chemistry and Natural Sciences* (Berlin: Springer Verlag)
[22] Hänggi P and Jung P 2007 *Adv. Chem. Phys.* **89** 239–326
[23] Dubkov A A, Spagnolo B and Uchaikin V V 2008 *Int. J. Bifurcation Chaos. Appl. Sci. Eng.* **18** 2649–72
[24] Janicki A and Weron A 1994 *Simulation and Chaotic Behavior of α-Stable Stochastic Processes* (New York: Marcel Dekker)
[25] Chechkin A V, Gonchar V Y, Klafter J and Metzler R 2006 Fundamentals of Lévy flight processes *Fractals, Diffusion, and Relaxation in Disordered Complex Systems: Advances in Chemical Physics, Part B* vol 133 ed T Coffey W and P Kalmykov Y (New York: John Wiley & Sons) pp 439–96
[26] Nolan J P 2020 *Univariate Stable Distributions* (New York, NY: Springer)
[27] Samorodnitsky G and Taqqu M S 1994 *Stable Non-Gaussian Random Processes: Stochastic Models with Infinite Variance* (New York: Chapman and Hall)
[28] Garbaczewski P and Stephanovich V 2011 *Phys. Rev.* E **84** 011142
[29] Chechkin A V, Klafter J, Gonchar V Y, Metzler R and Tanatarov L V 2003 *Phys. Rev.* E **67** 010102(R)
[30] Chechkin A V, Gonchar V Y, Klafter J, Metzler R and Tanatarov L V 2004 *J. Stat. Phys.* **115** 1505–35
[31] Shlesinger M F, Zaslavski G M and Klafter J 1993 *Nature (London)* **363** 31
[32] Klafter J, Shlesinger M F and Zumofen G 1996 *Phys. Today* **49** 33–9
[33] Solomon T H, Weeks E R and Swinney H L 1993 *Phys. Rev. Lett.* **71** 3975–8
[34] del Castillo-Negrete D 1998 *Phys. Fluids* **10** 576
[35] Chechkin A V, Gonchar V Y and Szydłowski M 2002 *Phys. Plasmas* **9** 78–88
[36] del Castillo-Negrete D, Carreras B A and Lynch V E 2005 *Phys. Rev. Lett.* **94** 065003
[37] Katori H, Schlipf S and Walther H 1997 *Phys. Rev. Lett.* **79** 2221–4
[38] Peng C K, Mietus J, Hausdorff J M, Havlin S, Stanley H E and Goldberger A L 1993 *Phys. Rev. Lett.* **70** 1343–6
[39] Segev R, Benveniste M, Hulata E, Cohen N, Palevski A, Kapon E, Shapira Y and Ben-Jacob E 2002 *Phys. Rev. Lett.* **88** 118102
[40] Lomholt M A, Ambjörnsson T and Metzler R 2005 *Phys. Rev. Lett.* **95** 260603
[41] Viswanathan G M, Afanasyev V, Buldyrev S V, Murphy E J, Prince P A and Stanley H E 1996 *Nature (London)* **381** 413–5
[42] Ditlevsen P D 1999 *Geophys. Res. Lett.* **26** 1441–4
[43] Mantegna R N and Stanley H E 2000 *An Introduction to Econophysics. Correlations and Complexity in Finance* (Cambridge: Cambridge University Press)
[44] Brockmann D, Hufnagel L and Geisel T 2006 *Nature (London)* **439** 462–5
[45] Kabašinskas A, Rachev S, Sakalauskas L, Sun W and Belovas I 2009 *J. Comput. Anal. Appl.* **11** 641–68
[46] Stoyanov S V, Samorodnitsky G, Rachev S and Ortobelli Lozza S 2006 *Probab. Math. Stat.* **26** 1–22
[47] Jas M, Dupré la Tour T, Simsekli U and Gramfort A 2017 *Adv. Neural. Inf. Process. Syst.* ed I Guyon *et al* (Curran Associates) 30 30, pp 1099–108
[48] Wang Z, Li Y, Xu Y, Kapitaniak T and Kurths J 2022 *J. Stat. Mech.* **2022** 053501
[49] Langevin P 1908 *C. R. Acad. Sci. (Paris)* **146** 530–3
[50] Sekimoto K 1998 *Prog. Theor. Phys. Suppl.* **130** 17–27
[51] Coffey W T and Kalmykov Y P 2012 The Langevin equation: with applications to stochastic problems *Physics, Chemistry and Electrical Engineering* (Singapore: World Scientific Publishing)
[52] Risken H *The Fokker-Planck Equation. Methods of Solution and Application* (Berlin: Springer Verlag)
[53] Dybiec B, Gudowska-Nowak E and Sokolov I M 2017 *Phys. Rev.* E **96** 042118
[54] Mantegna R N and Spagnolo B 1996 *Phys. Rev. Llett.* **76** 563
[55] Šiler M, Ornigotti L, Brzobohaty` O, Jákl P, Ryabov A, Holubec V, Zemánek P and Filip R 2018 *Phys. Rev. Lett.* **121** 230601
[56] Koren T, Lomholt M A, Chechkin A V, Klafter J and Metzler R 2007 *Phys. Rev. Lett.* **99** 160602–5
[57] Bier M 2018 *Phys. Rev.* E **97** 022113
[58] Capała K, Dybiec B and Gudowska-Nowak E 2020 *Chaos* **30** 013127
[59] Capała K, Padash A, Chechkin A V, Shokri B, Metzler R and Dybiec B 2020 *Chaos* **30** 123103
[60] Mercadier M, Guerin W, M Chevrollier M and Kaiser R 2009 *Nat. Phys.* **5** 602–5
[61] Barkai E, Aghion E and Kessler D A 2014 *Phys. Rev.* X **4** 021036–69
[62] Amor T A, Reis S D S, Campos D, Herrmann H J and Andrade J S 2016 *Sci. Rep.* **6** 20815
[63] Barthelemy P, Bertolotti J and Wiersma D 2008 *Nature (London)* **453** 495–8
[64] Fioriti V, Fratichini F, Chiesa S and Moriconi C 2015 *Int. J. Adv. Robot. Syst.* **12** 98
[65] Lera S C and Sornette D 2018 *Phys. Rev.* E **97** 012150

[66] Hall P 1981 *Bull. Lond. Math. Soc.* **13** 23–7
[67] Ditlevsen P D 1999 *Phys. Rev.* E **60** 172
[68] Imkeller P and Pavlyukevich I 2006 *Stoch. Proc. Appl.* **116** 611–42
[69] Imkeller P and Pavlyukevich I 2006 *J. Phys. A: Math. Gen.* **39** L237–46
[70] Getoor R K 1961 *Trans. Am. Math. Soc.* **101** 75–90
[71] Widom H 1961 *Trans. Am. Math. Soc.* **100** 252–62
[72] Kesten H 1961 *Illinois J. Math.* **5** 267–90
[73] Kesten H 1961 *Illinois J. Math.* **5** 246–66
[74] Zoia A, Rosso A and Kardar M 2007 *Phys. Rev.* E **76** 021116–26
[75] Bouchaud J P and Georges A 1990 *Phys. Rep.* **195** 127–293
[76] Chechkin A V, Sliusarenko O Y, Metzler R and Klafter J 2007 *Phys. Rev.* E **75** 041101
[77] Pavlyukevich I, Dybiec B, Chechkin A V and Sokolov I M 2010 *Eur. Phys. J. ST* **191** 223–37
[78] Hintze R and Pavlyukevich I 2014 *Bernoulli* **20** 265–81
[79] Higham D J 2001 *SIAM Rev.* **43** 525–46
[80] Mannella R 2002 *Int. J. Mod. Phys.* C **13** 1177–94
[81] Chambers J M, Mallows C L and Stuck B W 1976 *J. Am. Stat. Assoc.* **71** 340–4
[82] Weron A and Weron R 1995 *Lect. Not. Phys.* **457** 379–92
[83] Weron R 1996 *Statist. Probab. Lett.* **28** 165–71
[84] Kloeden P and Platen E 2011 *Numerical Solution of Stochastic Differential Equations Stochastic Modelling and Applied Probability* (Berlin: Springer Verlag)
[85] Widom H 1961 *Trans. Am. Math. Soc.* **98** 430–49
[86] Szczepaniec K and Dybiec B 2015 *J. Stat. Mech.* **2015** P06031–46
[87] Padash A, Chechkin A V, Dybiec B, Pavlyukevich I, Shokri B and Metzler R 2019 *J. Phys. A: Math. Theor.* **52** 454004